EMC and EMI issues of WPT systems for wearable and implantable devices

EMC and EMI issues of WPT systems for wearable and implantable devices

Giuseppina Monti, Diego Masotti, Giacomo Paolini, Laura Corchia, Alessandra Costanzo, Marco Dionigi, Franco Mastri, Mauro Mongiardo, Roberto Sorrentino, Luciano Tarricone

***Abstract*— This paper discusses the electromagnetic compatibility and interference aspects related to wireless power transfer systems for wearable and implantable devices. The cases of a near-field (reactive) link for recharging a pacemaker and a far-field (radiative) link for wearable devices are considered. For the first case a design approach, able to perform efficient energy transfer under the safety regulations constraints of medical devices is proposed. In the second case, a rigorous methodology is proposed to predict the transferred energy to a worn device able to account for interferences due to the human body or any other wireless system located close to the worn device. An implementation of grounded worn rectennas in the presence of unconventional radio channels is presented.**

***Index Terms*— radiative and non-radiative wireless power transfer, rectenna, electromagnetic compatibility, SAR, EM interference.**

I. INTRODUCTION

In all humanized environments a large set of wireless devices with communication and sensing capabilities is commonly present. The pervasive presence of "smart dust" [1] in any context of our daily life will rapidly increase, especially under the pressure of 5G-IoT emerging architectures [2]. The cut of wires in consumer and industrial applications involves different kinds of wireless power transfer (WPT) mechanisms, mainly dealing with near-field (NF) couplings and far-field (FF) transmission in such a way that most of the researchers' attention in the last decade is devoted to the maximization of the overall efficiency in the transfer operation [3-6], as well as to the regulations definition of the adopted protocols [7], when both NF and FF energy transfer mechanism are concerned. More recently, the problem of the Electromagnetic Compatibility (EMC) among different coexisting wireless devices/systems has drawn the attention of the scientific community: this is due to the twofold issue of human exposure [8-9] and of interference effects with the coexisting wireless electronic equipment caused by the electromagnetic field leakage [10-11]. The latter is increasingly important as the Simultaneous Wireless Power and Information Transfer (SWIPT) is one of the key features of future 5G architectures [12]: enabling a safe communication while transferring energy must rely on two completely uncoupled, though extremely closed, links [13-14].

As per problems related to human exposure, different scientific committees and international organizations care about EMC focusing on safety standards and associated risks: among the others, of particular relevance are the International Commission on Non-Ionizing Radiation Protection (ICNIRP) and the IEEE Standard Coordinating Committee 28 (SCC28) [8-9].

The inviolable limits are assessed appraising the values above which biological effects could appear. In this regard, two important variables to take into account are the Specific Absorption Rate (SAR), measured in W/kg, and the temperature variations of the involved tissues that could create the so called "thermal effects". SAR value can be assessed by estimating either its average value over the whole human body, or over a small mass of tissue, 10 g or 1 g, if the area involved is very localized.

A further important subject to consider if we talk about Wireless Power Transfer, both in NF and in FF, are the effects of the so called Electromagnetic Interference (EMI).

If the operating frequency of the power electronic system under examination is the same of the RF-to-RF WPT link, there is an emission of electromagnetic (EM) waves that could couple with the electronic devices, i.e. integrated circuits, of the same system [11]: this may lead to various complications, and results in the performance degradation of the embedded analog circuits [15-16]. The same situation occurs for the WPT technology using coupled-resonance, in the presence of which far-field emission becomes a cause of electromagnetic interference, in addition to power loss [17].

Another case of interference that can occur and has certainly to be minimized, is related to wireless data communication: in presence of unwanted EM fields: indeed, the data wireless channel could be partially or entirely disrupted, causing a critical loss of information of the whole information flow [18]. This review aims to address these targeted issues and to discuss possible theoretical and numerical approaches which can be adopted to rigorously model the associated effects.

Giuseppina Monti, Laura Corchia and Luciano Tarricone are with the Department of Engineering for Innovation, University of Salento, Lecce 73100, Italy (email: {giuseppina.monti, laura.corchia, luciano.tarricone}@unisalento.it).

Diego Masotti, Giacomo Paolini, Alessandra Costanzo and Franco Mastri are with the Department of Electrical, Electronic and Information Engineering 'Guglielmo Marconi', University of Bologna, Bologna, Italy (email: { diego.masotti, giacomo.paolini4, alessandra.costanzo, franco.mastri, }@unibo.it).

Marco Dionigi, Mauro Mongiardo and Roberto Sorrentino are with the Department of Engineering, University of Perugia, Perugia, Italy (email: {mauro.mongiardo, Roberto.sorrentino}@unipg.it).

doi: 10.1109/MEMC.0.8339550

For this purpose, the paper is organized as follows. In Section II the main figures of merit for characterizing NF- and FF-WPT links are introduced; in Section III a theoretical approach for the accurate evaluation of the performance of WPT links is discussed as a systematic approach to quantify the possible sources of interference for nearby wireless systems. Sections IV and V are dedicated to discuss few representative examples of application of WPT links when either implantable medical devices or wearable electronics are concerned. Finally, some conclusions are drawn in Section VI.

II. Figures of Merit of WPT Links

Solutions for NF- or FF-WPT exploit different electromagnetic mechanisms for transferring the energy [19], and usually involve different power levels and frequencies, as well as different space volumes: microwaves (300 MHz – 30 GHz) and millimetre-waves (30 – 300 GHz) are adopted when active radiation from antennas is received in the FF zone; conversely, low-frequency (LF: 30-300 kHz) and high-frequency (HF: 3-30 MHz) ranges are pertinent to reactive coupling between coils or plates. Thus, due to the completely different transmission mechanism, the covered distances and the interested volumes by the EM field are likewise different. In the FF-WPT the link distance ranges from few meters up to hundreds of kilometers, depending of course on the transmitted power level, which can be low (~mW) and high (~MW), respectively; the area, at the receiving side, exploiting the incoming EM field is typically small, because of the distance and the finite directivity of the antennas: as a consequence, a big amount of power could be lost in the FF transmission. In the NF case, the distance between the coils/plates can be from few millimeters to few centimeters, if a resonant condition is imposed (resonant NF-WPT), or up to tens of centimeters in the non-resonant NF-WPT; the narrowband behaviour of the resonant NF-WPT at both the transmitting and the receiving sides, makes the region interested by the resonant EM field extremely confined, thus drastically reducing the related EMC issues, and allowing the transfer of high levels of power (up to kW).

Despite of these differences, a unified approach for the design of these transferring systems is possible [20]. According to this approach, the figure of merit that a WPT system needs to maximize is the overall link efficiency, whose value results from the product of three efficiencies, according to the following expression:

$$\eta = \eta_{DC-RF} \cdot \eta_{RF-RF} \cdot \eta_{RF-DC} = \frac{P_{TX}}{P_{BIAS}} \cdot \frac{P_{RF}}{P_{TX}} \cdot \frac{P_{DC}}{P_{RF}} \qquad (1)$$

The first term is mainly related to the transmitting amplifier efficiency, thus taking into account how efficiently the DC power that is used to bias the nonlinear transistors (P_{BIAS}) is deployed to produce the high-frequency power to be transmitted (P_{TX}). The second factor takes into account the losses introduced by the wireless path (from few millimeters up to kilometers, depending on the WPT mechanism), and by the antennas/coils, being P_{RF} the power received by the antenna/coil: its accurate definition is particularly delicate, as well as important, in cases where lossy and dispersive media or non-conventional links are involved, such as for implantable devices and Body Area Network (BAN) applications, respectively. Finally, the RF-to-DC conversion efficiency (η_{RF-DC}) represents the quality factor of the rectifying section of the receiving side.

III. Accurate WPT Links Performance Evaluation

The accurate estimation of WPT systems efficiency (1) and, as a consequence, their effects on the surrounding environment and their reciprocal interference, is mainly dependent on the accurate evaluation of the RF power received by the rectenna (P_{RF}). This is of strategic importance in particular for those scenarios where harsh EM environments and/or ultra-low power levels are involved, such as in EMC issues for wireless nonlinear RF equipment operating in EM polluted ambient: a rough P_{RF} estimation can lead to highly erroneous predictions. Numerical approaches for the P_{RF}/interference evaluation can be developed from the rigorous application of the EM theory and the integration of different CAD techniques, in order to describe in the best way each part of the involved wireless link [21], and with increasing level of accuracy, depending on the environmental conditions.

A. Conventional Link Analysis

By referring to EMC/EMI problems, the simplest situation consists of a single-antenna wireless device receiving one interfering RF signal (at frequency f_{RF}) generated by an unintentional source of volume V_i and current density $\mathbf{J_i}$, placed in the far-field zone, in such a way that the incoming field ($\mathbf{E_i}$), in the wireless device location, can be considered as a uniform plane wave.

In these conditions, the receiving antenna can be viewed as a *linear active system*, and can be represented by a Norton equivalent circuit, as reported in Fig. 1: here, the single-port antenna is rigorously represented by its dispersive admittance, computed by EM analysis. In this way, the complete characterization of the receiving antenna is achieved by the further definition of the complex equivalent current generator $J_{eq}(f_{RF})$: the rigorous application of the reciprocity theorem [22] allows to reach the following formulation of the equivalent generator:

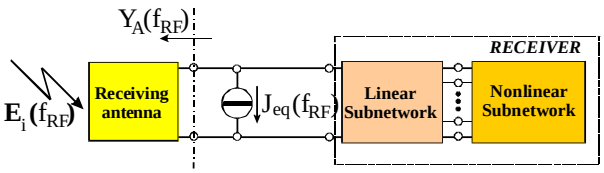

Figure 1. Block diagram of a single-antenna receiver under monochromatic incidence at frequency f_{RF}.

$$J_{eq}(f_{RF}) = \frac{1 + R_0 Y_A(f_{RF})}{U} \int_{V_i} \mathbf{J_i}(P_i) \bullet \mathbf{E_R}(P_i)\, dV_i \qquad (2)$$

where $\mathbf{E_R}$ represents the field radiated by the receiving antenna, when it works in transmitting mode, and is driven by a sinusoidal voltage source of frequency f_{RF}, electro-motive force U, and internal impedance R_0. Note that $\mathbf{E_R}$ can be easily

doi: 10.1109/MEMC.0.8339550

evaluated by means of a full-wave simulation. Despite of this, the direct exploitation of (2) is not straightforward, mainly because of the RF source current density evaluation. By resorting again to the EM theory, (2) can be expressed by the following simpler formula, provided that the hypothesis of uniform plane wave is valid [23]:

$$J_{eq}(f_{RF}) \approx j\left[1+R_0 Y_A(f_{RF})\right] \frac{2\lambda_{RF}\, r\, e^{j\beta r}}{\eta} \frac{\mathbf{E_i} \bullet \mathbf{E_R}(\theta_L, \phi_L)}{U} \qquad (3)$$

where $\mathbf{E_R}(\theta_L, \phi_L)$ is the field radiated by the receiving antenna in the link direction (θ_L, ϕ_L), but evaluated in the far-field zone at a distance r from the phase center of the RF source antenna, and η, β are the free-space wave impedance and phase constant, respectively.

The approximation of (3) depends on both phase and amplitude errors introduced by adopting (1), thus by considering a spherical wave as a uniform plane one. These errors can be quantified by simple geometrical considerations: the "plane" and "uniform" approximations are responsible for a phase error $o(D^2/\lambda_{RF}r)$ and an amplitude error $o(D^2/r^2)$, respectively, where D is the receiving antenna size. These errors are both negligible under the assumption of far-field condition satisfied. One can note that the amplitude error behaviour is valid only if the receiver is located along the direction of maximum radiation of the transmitting antenna: if this condition is not valid, the error can become significant, depending on the transmitting antenna radiation pattern.

Once the equivalent current is evaluated by (3), the "active" receiving device is described as in Fig. 1 and its circuit analysis can be straightforwardly carried on. The Harmonic Balance (HB) technique has demonstrated to be the most suitable method for RF circuit analysis, in the last decades [24]: the description of the linear subnetwork (antenna and its feeding network) and of the nonlinear one (receiving circuitry) in the frequency and time domain, respectively, is the key feature of an HB-based simulation. In the case under exam, a sinusoidal analysis involving a number (e.g., n_H) of the fundamental frequency harmonics ($k \cdot f_{RF}$, k=0, 1,...,n_H,) can be easily carried on.

B. Non-conventional Link Analysis

In many applications, the reciprocal positions of transmitting RF source and receiving device are such that the phase and/or the amplitude errors cannot be neglected: this could mean that the two antennas/coils are not in the far-field region of each other (i.e. the interfering transmitted signal is generated by a neighboring wireless device, or by another part of the same circuit, providing an unintentional radiation due to high frequency signals involved, or the two coils exploit reactive fields in the near-field region), or the link direction is far from being the maximum radiation direction (i.e. in a wearable wireless device for BAN or energy harvesting applications). In this more general situation, the Norton equivalent generator of Fig. 1 cannot be evaluated through (3). However, the accurate estimation of this contribution is of fundamental importance, especially in those cases where low-power levels are involved, as in EMC/EMI problems, or in RF energy harvesting from environmental sources. For these reasons, a rigorous evaluation of J_{eq} under general conditions has been proposed, too [25]. According to this approach, an alternative and equivalent formulation of (2) can be reached through the standard application of the field equivalence theorem, thus replacing the 3D current density $\mathbf{J_i}$ on V_i with the equivalent surface currents (both electric and magnetic), due to the electromagnetic field ($\mathbf{E_i}$, $\mathbf{H_i}$) generated by $\mathbf{J_i}$, evaluated on the surface S of an infinite plane placed in between the two (transmitting and receiving) antennas:

$$\begin{aligned} &J_{eq}(f_{RF}) = \\ &= \frac{1+R_0 Y_A(f_{RF})}{U} \int_S \left(\mathbf{J_{surf}}(P_S) \bullet \mathbf{E_R}(P_S) - \mathbf{M_{surf}}(P_S) \bullet \mathbf{H_R}(P_S)\right) dS = \\ &= \frac{1+R_0 Y_A(f_{RF})}{U} \bullet \hat{\mathbf{n}} \bullet \int_S \left[\mathbf{E_i}(P_S) \times \mathbf{H_R}(P_S) - \mathbf{E_R}(P_S) \times \mathbf{H_i}(P_S)\right] dS \end{aligned} \qquad (4)$$

where the symbols share the same meaning of (3) (for the magnetic field, too), P_S and $\hat{\mathbf{n}}$ are a generic point and the unit vector orthogonal to the surface S, respectively (Fig. 2).

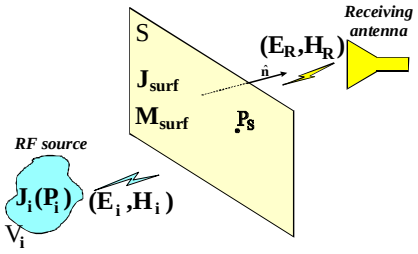

Figure 2. Set-up for the rigorous evaluation of (4) for both FF and NF applications.

The new formulation of J_{eq} is now rigorous, and its evaluation can be performed by resorting to two full-wave simulations, one for each antenna: the outputs of each analysis are the EM fields appearing in (4), evaluated on a surface S placed in between the actual position of the antennas. The relative difference in the magnitude of J_{eq} given by (3) and (4) can reach the 50% in those critical scenarios, where low amount of power are involved and both the distance and orientation of the two antennas make the plane wave approximation too simplistic [25], thus drastically affecting the $\eta_{RF\text{-}DC}$ estimation in (1). After the evaluation of (4), considerations similar to those mentioned in the previous sub-section hold for the HB analysis of the "active" receiving circuit represented in Fig. 1.

An increased level of complexity is represented by the presence of a multi-port (e.g., R) antenna in the receiving wireless device: this is the case of RF energy harvesting systems for low-power density scenarios, where both two differently aligned antennas or multi-antenna architectures are able to increase harvested power [26]; or in EMI case where each nonlinear device of a circuit can be viewed as a potential receiver of unwanted signals [23]; or in EMC case, where different receiving neighboring devices exploiting spatial diversity and operating at the same frequency (e.g. in MIMO systems) are invested by an interfering signal [26]. From the circuital point of view, this situation is described by the

doi: 10.1109/MEMC.0.8339550

scheme of Fig. 3: the $\mathbf{Y_A}$ is now an RxR matrix, thus taking into account all the EM couplings between the different ports of the multi-port receiving antenna.

The most significant difference with respect to the previous cases is the evaluation of the equivalent current generator: in fact, referring to the p-th port of the multi-port antenna, (1) is replaced by:

$$J_{eq}^{(p)}(f) = \frac{1 + R_0 Y_{pp}(f)}{U} \int_{V_i} \mathbf{J_i}(P_i) \bullet \mathbf{E_R^{(p)}}(P_i)\, dV_i \qquad (5)$$

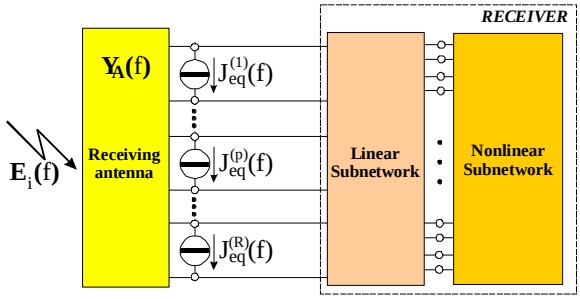

Figure 3. Block diagram of a multi-antenna receiver under monochromatic incidence at frequency f.

where both the admittance (Y_A) and the radiated field of the standalone antenna ($\mathbf{E_R}$) of (2) are now replaced by the admittance Y_{pp} and the radiated field $\mathbf{E_R^{(p)}}$ of the p-th port involved in the calculation. Of course, the main consequence of this difference relies on the effects that the transadmittances Y_{pm} ($m \neq p$) have on the p-th port of the antenna (automatically included in the Y_{pp} value). This fact has proven to have significant effects in cases where the multi-antenna solution needs for close ($< \lambda/10$) placement of the antennas, e.g. multi-rectenna with differently polarized close antennas, or in EMI cases where the ports of each nonlinear device of the receiving system can be coupled with the ports of the other devices [23].

The evaluation of (5) can be obtained by adopting (3) or (4) depending on the reciprocal position between the single source and each antenna/coil of the receiving device. The HB-analysis in this case is identical to the previous ones from the regime point of view (single tone analysis); it becomes simply more time- and memory-consuming due to the higher number of nonlinear devices involved in the multi-port receiving subsystem. An additional increase of complexity is represented by the simultaneous presence of several incoming fields at different frequencies ($f_{RF,k}$) : the evaluation of (3), (4), (5) has to be carried out at each frequency and the corresponding HB simulation becomes a multi-tone one.

IV. THE CASE OF A NEAR-FIELD LINK FOR RECHARGING A PACEMAKER

A possible attractive application of the WPT technology is the recharge of implantable medical devices (IMDs) [27]-[30].

Nowadays, IMDs are increasingly used for the treatment of important diseases, such as cardiac pathologies, chronic pain, essential tremor from Parkinson's disease, etc.

Most of these devices, see the case of pulse generators for cardiac and deep brain stimulation, are powered by a battery and have a limited lifetime. For instance, pacemakers have a lifetime which depends on the pathology to be treated and varies between 2 and 10 years.

In recent years, the use of WPT as a viable solution for lengthening the lifetime of these devices has been demonstrated [31] – [40].

The basic idea is to replace the traditional battery of the IMD with a rechargeable one and to use a WPT link between an implanted receiver and an external transmitter to periodically recharge the battery (see Fig. 4).

With respect to conventional WPT systems operating in free-space, the design of a WPT link aiming at recharging an IMD has to face two main issues.

The first issue is related to the presence of the biological tissues which are lossy and can degrade the RF-to-RF power transfer efficiency of the link.

The second issue is the EMC of the link: the WPT link has to be designed in order to allow the recharge of the IMD in a reasonable charging time and in compliance with the limits imposed by safety regulations.

Usually, in order to minimize problems related to both the above described issues, WPT links for IMDs are usually based on an inductive (possibly resonant) non-radiative coupling [31]-[40]. In fact, for the specific application, transfer distances from few millimeters up to some centimeters are sufficient; additionally, the use of a magnetic coupling allows minimizing the interaction with human tissues.

In the following part of this section the case of the WPT link for recharging a pulse generator for cardiac stimulation presented in [40] is analyzed with particular emphasis on EMC issues.

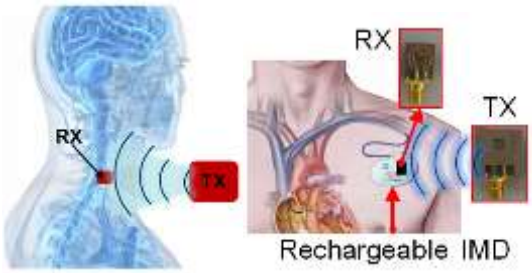

Figure 4. Examples of WPT links for recharging a medical implant: the WPT occurs between an exeternal transmitter and an implanted receiver.

A. *Resonant Inductive Link for a rechargeable pacemaker*

The considered WPT link is the one presented in [40]. It consists of two magnetically coupled resonators. Considering that pacemakers are implanted at a few millimeters under the skin, the link is configured for optimal operation with the primary resonator in direct contact with the skin and the receiving resonator integrated into the silicon header of a pacemaker (the Vitatron T60 DR pacemaker has been taken as a reference, see Fig. 5) and implanted at a depth of 5 mm. The operating frequency is 403 MHz, i.e., at the central frequency of the MedRadio (Medical Device Radiocommunications Service) band reserved to medical devices.

doi: 10.1109/MEMC.0.8339550

Each resonator consists of a planar loop loaded by a lumped capacitor, the fabricated prototypes are illustrated in Fig. 6.

The performance calculated by full-wave simulations, performed by taking into account the presence of the human tissues (a thickness of 2 mm is assumed for both the fat and the skin layers, see Fig. 5), are given in Fig. 7. The results obtained by using a normalization impedance of 50 Ω are reported. By exploiting the frequency-based scattering parameter values, the calculated efficiency at 403 MHz is about 57 % (see Fig. 8). These results have been experimentally verified by using a minced of pork to simulate the presence of the human tissues (see Fig. 6). Experimental results are given in Figs. 7-8 and are compared with numerical data. As it can be seen from Fig. 7, a reasonable agreement between experimental and simulated data has been obtained for the S_{21} and the S_{11} parameters; while, the agreement is worse for the S_{22} parameter. This is likely due to the presence of air sacs between the pacemaker and the minced of pork.

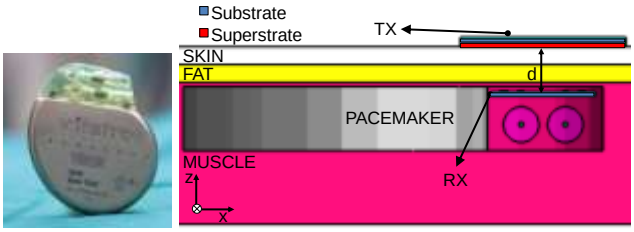

Figure 5. Vitatron T60 DR pacemaker assumed as a reference for the dimensions of the pacemaker (on the left) and configuration of the WPT link for the recharge of a pacemaker (on the right).

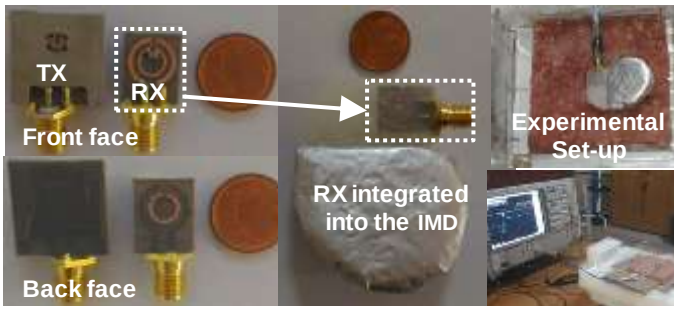

Figure 6. Fabricated prototype. The central photograph shows the prototype fabricated for simulating the integration of the receiver into the silicon header of a Vitatron T60 DR pacemaker.

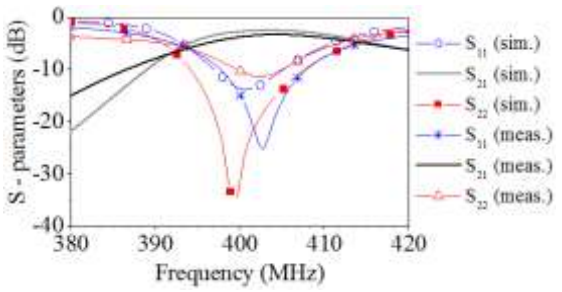

Figure 7. Scattering parameters of the link illustrated in Figs. 5-6: comparison between simulated and measured data.

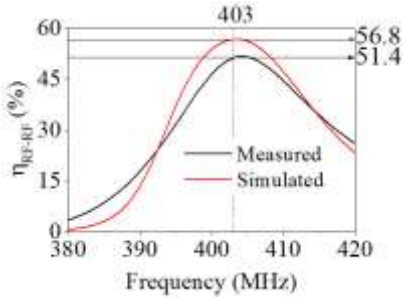

Figure 8. RF-to-RF power transfer efficiency of the link illustrated in Figs. 5-6: comparison between simulated and measured data.

Assuming that, the link is connected to a generator having an input impedance of 50 Ω and to a load of 50 Ω, the RF-to-RF power transfer efficiency of the link can be calculated from the scattering parameters as follows:

$$\eta_{RF-RF} = |S_{21}|^2 \quad (6)$$

where $|S_{21}|$ is the transmission coefficient of the link normalized with respect to 50 Ω. The results obtained from full-wave simulations and mesurements are given in Fig. 8; the RF-to-RF conversion efficiency measured at 403 MHz is approximately equal to 51 %.

B. Achievable Performance and Compliance With Safety Regulations

Modern pacemakers use a lithium-ion (Li-ion) battery with a capacity in the range of [0.5, 325] mAh. A WPT link intended for recharging these medical implants should be able to recharge the device in a reasonable charging time (T_{charge}) and in compliance with safety regulations.

These aspects are discussed in the following part of this subsection.

1) Achievable performance

In order to discuss the aspects related to EMC issues for the WPT link of Fig. 6, it is first of all necessary to assess the achievable performance for a charger using the link.

A schematic representation of a possible implementation of a wireless battery charger for Li-ion batteries is illustrated in Fig. 9.

The wireless charger consists of two main blocks: 1) the RF-to-RF wireless link, 2) the RF-to-DC converter.

In particular, the RF-to-DC converter substantially consists of: 1) a rectifier which converts the RF signal at the output port of the receiver of the RF-to-RF wireless link into a DC signal, and 2) a DC-to-DC converter which converts the rectified DC signal into a DC signal suitable to be used for recharging the battery.

According to the schematic representation illustrated in Fig. 9, the overall efficiency of the wireless charger can be calculated as a product of the efficiencies of each sub-block:

$$\eta_{TOT} = \frac{P_{BATT}}{P_G} = \left(\frac{P_{BATT}}{P_{RF}}\right) \times \left(\frac{P_{RF}}{P_G}\right) = \eta_{RF-DC} \times \eta_{RF-RF} \quad (7)$$

With regard to Li-ion batteries, the typical value that can be realized for η_{RF-DC} is in the range of [70 - 90] % , [41]-[43].

doi: 10.1109/MEMC.0.8339550

Accordingly, it can be concluded that for a charger using the RF-to-RF wireless link of Fig. 6, which has a measured efficiency of about 51%, values of the overall efficiency in the range [36 - 46] % can be reasonably realized.

Additionally, with regard to lithium technology, it should be considered that in order to lengthen the lifetime of the battery a good practice is to recharge the battery when its charge is 20 % below the maximum level. Accordingly, assuming a charging current I_{charge}, the time necessary for recharging a battery with a capacity C is:

$$T_{charge} = \frac{C}{I_{charge}} \times 0.2 \tag{8}$$

For the analyzed case I_{charge} can be expressed as:

$$I_{charge} = \eta_{TOT} \times P_G \times \frac{1}{V_{charge}} \tag{9}$$

Accordingly, the maximum value of the capacity of a battery which can be recharged in a charging time T_{charge} by using the wireless charger of Fig. 9 is:

$$C_{max} = \eta_{TOT} \times P_G \times \frac{1}{V_{charge}} \times T_{charge} \times \frac{1}{0.2}, \tag{10}$$

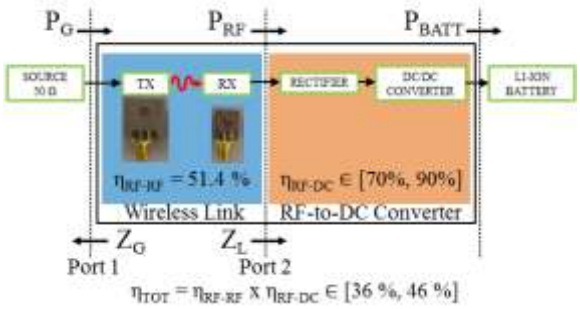

Figure 9. Schematic representation of a wireless battery charger.

where, the maximum value usually assumed by V_{charge} is 4.1 V. Equation (10) highlights that, for given values of η_{TOT} and T_{charge}, C_{max} depends on P_G which in turn depends on the limits imposed by safety regulations.

2) Compliance with safety regulations

In the MedRadio band, safety guidelines on exposure to electromagnetic fields provide restrictions in terms of the Specific Absorption Rate (SAR) [44], [45]. SAR is a measure of the rate at which energy is absorbed by a biological system when exposed to RF electromagnetic fields and can be expressed as the time derivative of the incremental energy dW absorbed by an incremental mass dm in an infinitesimal volume element dV of a given density ρ:

$$SAR = \frac{\partial}{\partial t}\frac{dW}{\rho dV} \tag{11}$$

For a lossy dielectric with electrical conductivity σ and exposed to an electric field E, the following expression can be derived:

$$SAR = \frac{\sigma |E|^2}{2\rho} \tag{12}$$

The energy absorbed by a lossy medium determines an increase of the temperature T, the SAR quantifies this heating effect and can be also expressed as: $SAR = \partial T / \partial t$.

Current guidelines impose limits on the peak SAR averaged on a reference mass (SAR_{rm}) of tissue (rm), typically 1-g or 10-g [44], [45] (i.e., the peak spatial-averaged SAR).

In particular, for the trunk area the exposure limit imposed by the Federal Communications Commission (FCC) guidelines, is 1.6 W/kg for the SAR_{1g}; while, the limit imposed by the ICNIRP is 2 W/kg for the SAR_{10g}.

SAR_{rm} is usually numerically estimated by using dedicated algorithms and several commercial tools are available for the calculation. In particular, the simulator CST Microwave Studio (MS) allows the calculation of both the SAR_{1g} and the SAR_{10g}. Considering that, for the trunk area the more stringent limit is that imposed by the FCC, full-wave simulations were performed for calculating the SAR_{1g}. The calculation has been performed by varying the value of the power provided to the primary resonator, P_G, in the range of [10 – 18] mW; the obtained results are summarized in Fig. 10. The red continuous line is the SAR_{1g}; while, the triangles are the values of the maximum capacity of a lithium battery, C_{max}, which can be recharged for different values of P_G. In calculating C_{max}, the realistic value of 80% has been assumed for $\eta_{RF\text{-}DC}$. As per T_{charge}, the reported values refer to a charging time of 6 hours.

From Fig. 10 it is evident that values of the SAR_{1g} below the limit of 1.6 W/kg have been obtained for P_G <13 mW; the SAR distribution achieved for P_G =13 mW is given in Fig. 11. From Fig. 10 it is also evident that a value of 13 mW for P_G corresponds to a value for the maximum capacity which can be recharged of about 40 mAh.

Finally, it is worth investigating the temperature rising (ΔT) associated to a single recharge cycle. The results calculated by the full-wave simulator CST MS are given in Fig. 12; for each of the three tissues affected by the power transfer, the figure shows the temperature rise in the point corresponding to the maximum value calculated for the SAR_{1g}. As expected, the maximum value of ΔT has been calculated for the skin layer and it is equal to 0.36 °C. According to the results reported in Figs. 10-12, it can be inferred that the link is compliant with safety regulations when used for recharging a battery with a capacity lower than 40 mAh.

In this regard, it is worth observing that the limit assumed in this paper is the one which applies for public exposure, which is far more stringent than that which applies for occupational exposure (for instance, for occupational exposure, the limit imposed by FCC guidelines on the SAR_{1g} is 8 W/kg).

However, to the best knowledge of the authors, there are no specific guidelines on which limits apply for the application here considered, i.e. the wireless recharging of a medical implant, and therefore, for the sake of providing an example, the most stringent limit has been here considered.

doi: 10.1109/MEMC.0.8339550

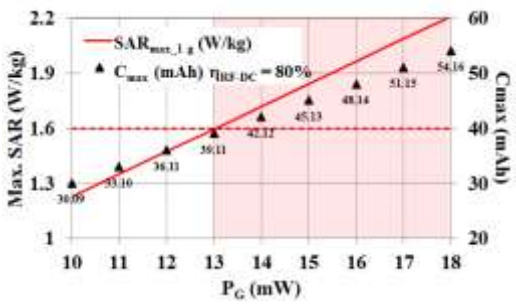

Figure 10. SAR_{1g} calculated for different values of PG (continous red line). The triangles are the maximum values of the capacity which can be recharged in a charging time of 6 hours in the case where $\eta_{RF\text{-}DC}$ is equal to 80 %. The red dashed line is the limit imposed by safety regulations for the SAR_{1g}.

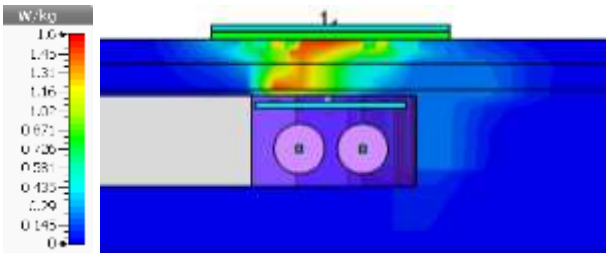

Figure 11. SAR_{1g} distribution calculated for P_G = 13 mW.

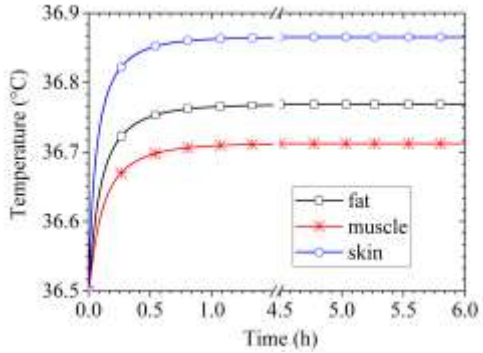

Figure 12. Temperature rise behaviour obtained for P_G equal to 13 mW.

V. THE CASE OF A FAR-FIELD LINK FOR WEARABLE RECTENNAS

The case of wearable rectifying antennas (rectennas) for RF energy harvesting purposes is an example of application where the rigorous approach described in Section II is mandatory. The ultra-low level of the involved signals forces to be extremely accurate in the evaluation of the RF power received by the rectenna and made available at the rectifier input port (P_{RF}), according to the generic scheme of a rectenna system reported in Fig. 13.

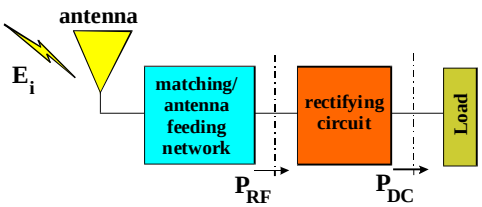

Figure 13. Block diagram of an RF energy harvesting system.

In presence of a wearable device the EMC/EMI issue has to be carefully taken into account, too. As an example of such a design, the three-band wearable rectenna proposed in [46] is considered; the envisaged application is the realization of special garments in harsh EM environments (e.g. firefighters).

The design start, of course, from the EM characterization of the selected fabrics: common 4 mm-thick pile for the antenna substrate and a 70 μm-thick Flectron conductive fabric. By means of resonant methods [46] it is possible to retrieve the pile characteristics (ε_r = 1.23, tanδ=0.0019 @ 2 GHz), whereas the conductive fabric results to have high conductivity (~1e+7 S/m) and, most of all, minimal fraying during manufacturing. The exploded view of the final rectenna layout is shown in Fig. 14, where the sole non-wearable part is the yellow one, consisting of a 100 μm-thick flexible Kapton (ε_r = 3.4, tanδ = 0.002 @ 10 GHz) for the antenna matching/feeding circuitry.

As regards the antenna selection, it is an annular ring with inner and outer radii of 21 mm and 71 mm, respectively. The proper placement of cuts in the antenna metallization allows to tune the operating frequencies of three resonant modes in correspondence of the desired frequencies: mode TM11@900 MHz, mode TM21@1800 MHz, mode TM12@2.45 GHz. Another grounded pile substrate is attached behind the Kapton layer to act as an additional shield: this solution prevents from back radiation into the human tissues for EMC reasons and increases the antenna gain, especially thanks to the possibility to make the shield large (e.g. when the rectenna is placed in the back of the technical jacket).

Note that the circular polarization is an additional goal of this project, because the reciprocal position of transmitting RF source and receiving rectenna is not a priori known: therefore the annular ring has two ports, corresponding to the two feeding microstrip lines in the lower Kapton layer, EM-coupled with the antenna through two orthogonal apertures obtained from the Kapton ground plane. Figure 15 shows in detail the layout of the Kapton circuitry [45], where the broadband 90° phase-shifter is also included for proper excitation of the orthogonal modes for circular polarization purposes.

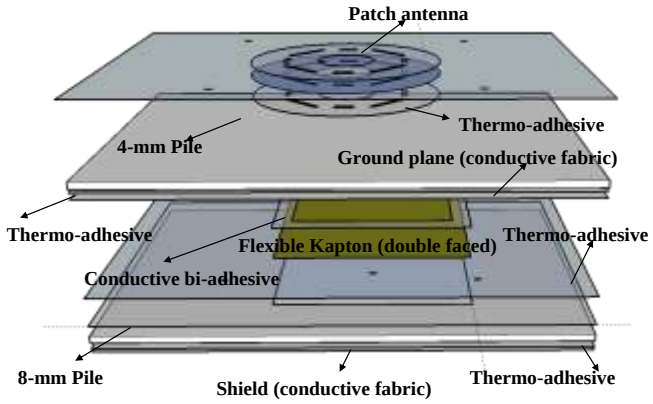

Figure 14. Exploded view of a fully wearable three-band energy harvester.

doi: 10.1109/MEMC.0.8339550

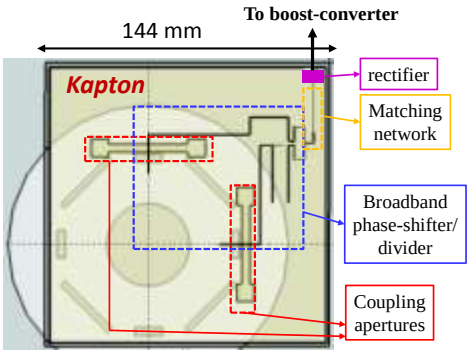

Figure 15. Detailed view of the feeding network of the rectenna of Fig. 14.

The layout of the feeding network is the result of an HB-based three-tone optimization, where three Norton equivalent current generators have been placed at the unique port of the EM-based description of the antenna/feeding network sub-assembly, according to the scheme of Fig. 1.

As validation of the design strategy, a worn prototype has been tested in an indoor scenario at the three operating frequencies at a time: first, the measured received P_{RF} is compared with predictions provided by (4). The use of this formula (instead of (3)) is justified by the inclusion of a portion of human body and a slight bending of the antenna (corresponding to an average chest curvature) in the EM simulation of the receiving system, and by the non-perfect alignment between the RF source (TDK-HRN0118 horn antenna) and the harvester. The simulation results are shown in Fig. 16, showing a very good agreement with measurements, despite of the real laboratory scenario full of furniture: the channel effect, not considered in the estimation, is responsible for the 20% difference at the lower frequency, only.

The second experiment is related to the complete rectenna prototype, including the Power Management Unit (PMU) instead of the fixed load of Fig. 13. The PMU's task is to emulate a loading condition corresponding to the maximum rectified power point, for each incoming power level and frequency [46]. The complete worn rectenna is now placed at 1 m distance from a mobile phone adopting the GSM 900 MHz frequency. Figure 17 reports the time-based waveform of the rectified voltage across the storage capacitor at the output port of the PMU, i.e. the port directly connected to the final user (e.g. a sensor), during a common phone call. A stored DC voltage of ~600 mV is reached in 3 s and the average RF received power is estimated as ~80 μW.

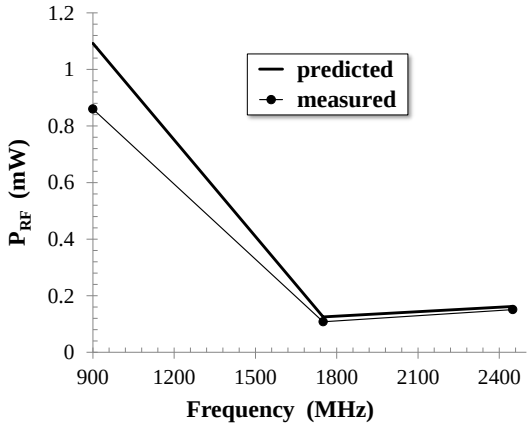

Figure 16. Predicted and measured available powers at the rectifier input port.

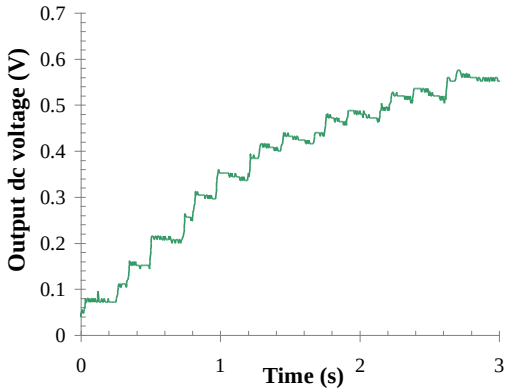

Figure 17. Voltage waveform at the storage capacitor terminals during a GSM900 phone call.

VI. Conclusion

The need for the accurate estimation of the wireless link performance for data end energy transfer is mandatory for estimating the related EMC issues, both in the near-field and in the far-field power transfer cases: when the radio channel consists of the presence of a complex media (as for implantable devices) and/or harsh electromagnetic environments (as in industrial sites) and/or misalignment between antennas/coils (in non-conventional far-field links or near-field couplings) this evaluation cannot rely on approximate formulations and indeed is a cumbersome problem. For these reasons, the combination of EM theory, full-wave analysis, and nonlinear circuit-based techniques (such as Harmonic Balance) into a Computer-Aided Design platform becomes a must to predict in a meaningful way EMI and EMC of the ambient involved. The effectiveness of the proposed integrated design approach is validated in this work by means of selected significant examples both in the reactive near-field case and in the radiative far-field one, when low amount of power is available, thus when the accurate estimation of the energy involved is crucial for the effective exploitation of the whole system technology: the predicted and experimentally validated performance of representative realized prototypes for energizing an implantable device and for realizing a wearable multi-band energy harvester

doi: 10.1109/MEMC.0.8339550

demonstrates the accuracy of the proposed analysis and design strategy.

REFERENCES

[1] Smart dust: Communicating with a cubic-millimeter computer B Warneke, M Last, B Liebowitz, KSJ Pister - Computer, 2001.

[2] M. R. Palattella *et al*., "Internet of Things in the 5G Era: Enablers, Architecture, and Business Models," *IEEE Journal on Selected Areas in Communications*, vol. 34, no. 3, pp. 510-527, March 2016.

[3] "Europe and the Future for WPT : European Contributions to Wireless Power Transfer Technology," in *IEEE Microwave Magazine*, vol. 18, no. 4, pp. 56-87, June 2017.

[4] A. Costanzo, D. Masotti, "Wirelessly powering: An enabling technology for zero-power sensors, IoT and D2D communication," *2015 IEEE MTT-S International Microwave Symposium*, Phoenix, AZ, 2015, pp. 1-4.

[5] O. Galinina, H. Tabassum, K. Mikhaylov, S. Andreev, E. Hossain and Y. Koucheryavy, "On feasibility of 5G-grade dedicated RF charging technology for wireless-powered wearables," *IEEE Wireless Communications*, vol. 23, no. 2, pp. 28-37, April 2016.

[6] F. Mastri, A. Costanzo and M. Mongiardo, "Coupling-Independent Wireless Power Transfer," *IEEE Microwave and Wireless Components Letters*, vol. 26, no. 3, pp. 222-224, March 2016.

[7] Applications of wireless power transmission via radio frequency beam - Report ITU-R SM.2392-0 (https://www.itu.int/md/R15-SG01-C-0025).

[8] A. Christ, M. Douglas, J. Nadakuduti and N. Kuster, "Assessing Human Exposure to Electromagnetic Fields From Wireless Power Transmission Systems," in *Proceedings of the IEEE*, vol. 101, no. 6, pp. 1482-1493, June 2013.

[9] A. Christ *et al*., "Evaluation of Wireless Resonant Power Transfer Systems With Human Electromagnetic Exposure Limits," in *IEEE Transactions on Electromagnetic Compatibility*, vol. 55, no. 2, pp. 265-274, April 20.

[10] Y. Kanasaki *et al*., "Analysis of electromagnetic field leaked from several Wireless Power Transfer Systems in large-scale model," *2016 IEEE Wireless Power Transfer Conference (WPTC)*, Aveiro, 2016, pp. 1-3.

[11] S. Kong *et al*., "An Investigation of Electromagnetic Radiated Emission and Interference From Multi-Coil Wireless Power Transfer Systems Using Resonant Magnetic Field Coupling," in *IEEE Transactions on Microwave Theory and Techniques*, vol. 63, no. 3, pp. 833-846, March 2015.

[12] E. Hossain, M. Rasti, H. Tabassum, A. Abdelnasser, "Evolution toward 5G multi-tier cellular wireless networks: An interference management perspective," *IEEE Wireless Communications*, vol.21, no.3, pp.118-127, June 2014.

[13] M. Fantuzzi, D. Masotti, A. Costanzo, "A Novel Integrated UWB–UHF One-Port Antenna for Localization and Energy Harvesting," *IEEE Trans. on Antennas and Propagation*, vol. 63, no. 9, pp. 3839-3848, Sept. 2015.

[14] M. Del Prete, F. Berra, A. Costanzo, D. Masotti, "Seamless Exploitation of Cell-phone Antennas for Near-field WPT by a Frequency-diplexing Approach", *IET Microwaves Antennas & Propagation*, Vol. 11, no. 5, 2016, pp. 649 – 656.

[15] J. Kim *et al.*, "Effects of on-chip and off-chip decoupling capacitors on electromagnetic radiated emission," in *IEEE Electron. Compon. Technol. Conf.*, Seattle, WA, USA, May 25–28, 1998, pp. 610–614.

[16] J. S. Pak, J. Lee, H. Kim, and J. Kim, "Prediction and verification of power/ground plane edge radiation excited by through-hole signalvia based on balanced TLM and via coupling model," in Elect. Perform.Electron. Packag., Princeton, NJ, USA, Oct. 27–29, 2003, pp. 181–184.

[17] H. Hirayama, T. Amano, N. Kikuma and K. Sakakibara, "Undesired emission and biological effect of open-end and short-end antennas for coupled-resonant wireless power transfer," *2013 Asia-Pacific Symp. on Electromagnetic Compatibility (APEMC)*, Melbourne, VIC, 2013, pp. 1-4.

[18] E. N. Baikova, S. S. Valtchev, R. Melício and V. F. Pires, "Wireless power transfer impact on data channel," *2016 Int. Symp. on Power Electronics, Electrical Drives, Automation and Motion (SPEEDAM)*, Anacapri, 2016, pp. 582-587.

[19] A. Costanzo and D. Masotti, "Energizing 5G: Near- and Far-Field Wireless Energy and Data Transfer as an Enabling Technology for the 5G IoT," *IEEE Microwave Magazine*, vol. 18, no. 3, pp. 125-136, May 2017.

[20] A. Costanzo, M. Dionigi, D. Masotti, M. Mongiardo, G. Monti, L. Tarricone, R. Sorrentino, "Electromagnetic Energy Harvesting and Wireless Power Transmission: A Unified Approach," *Proceedings of the IEEE*, vol.102, no.11, pp.1692,1711, Nov. 2014.

[21] V. Rizzoli, A. Costanzo, D. Masotti, M. Aldrigo, F. Donzelli, V. Degli Esposti., "Integration of non-linear, radiation, and propagation CAD techniques for MIMO link design", *Int. Journal of Microwave And Wireless Technologies*, Apr. 2012, Vol 4 No.2., pp. 223-232.

[22] R. F. Harrington, Time-Harmonic Electromagnetic Fields. New York: McGraw-Hill, 1973.

[23] V. Rizzoli, A. Costanzo, and G. Monti, "General electromagnetic compatibility analysis for nonlinear microwave integrated circuits", *2004 IEEE MTT-S Int. Microwave Symp. Digest*, Fort Worth, TX, June 2004, pp. 953-956.

[24] A. Costanzo, D. Masotti, M. Fantuzzi, M. Del Prete, "Co-Design Strategies for Energy-Efficient UWB and UHF Wireless Systems," *IEEE Trans. on Microwave Theory and Techn.*, vol. 65, no. 5, pp. 1852-1863, May 2017.

[25] A. Costanzo, A. Romani, D. Masotti, N. Arbizzani, V. Rizzoli, "RF/baseband co-design of switching receivers for multiband microwave energy harvesting", *Elsevier Journal on Sensors and Actuators A: Physical*, Mar. 2012, Vol. 179, No. 1, pp. 158-168.

[26] Z. Popović *et al.*, "Scalable RF Energy Harvesting," *in IEEE Trans. on Microwave Theory and Techniques*, vol. 62, no. 4, pp. 10461056, April 2014.

[27] J. S. Ho *et al*., "Wireless power transfer to deep-tissue microimplants", *Proc. Nat. Acad. Sci. USA*, vol. 111, no. 22, pp. 7974-7979, Apr. 2014.

[28] M. K. Hosain *et al.*, "Development of a Compact Rectenna for Wireless Powering of a Head-Mountable Deep Brain Stimulation Device," *IEEE Journ. of Translational Engineering in Health and Medicine*, vol.2, pp.1-13, Apr. 2014.

[29] P. Li and R. Bashirullah, "A Wireless Power Interface for Rechargeable Battery Operated Medical Implants," *IEEE Trans. Circuits Systems*, vol. 54, no. 10, pp. 912-916, Oct. 2007.

[30] X. Qi et al., "Batteries Not Included: A Mat-Based Wireless Power Transfer System for Implantable Medical Devices As a Moving Target," *IEEE Microwave Magazine*, vol. 14, no. 2, pp. 63-72, Mar.-Apr. 2013.

[31] K. Jung *et al.*, "Wireless Power Transmission for Implantable Devices Using Inductive Component of Closed-Magnetic Circuit Structure," in *Proc. IEEE Intern. Conf. Multis. Fusion Integr. Intell. Syst.*, Seoul, 2008, pp. 272-277.

[32] U. M. Jow and M. Ghovanloo, "Modeling and optimization of printed spiral coils in air, saline, and muscle tissue environments," *IEEE Trans. Biomed. Circuits Systems*, vol. 45, no. 1, pp. 21-22, Aug. 2009.

[33] G. Monti, L. Tarricone, and C. Trane, ''Experimental characterization of a 434 MHz wireless energy link for medical applications,'' in *Progress in Electromagn. Research C*, vol. 30, pp. 53–64, May 2012.

[34] G. Yilmaz, and C. Dehollaini, "An efficient wireless power link for implanted biomedical devices via resonant inductive coupling," in *IEEE Radio and Wireless Symposium (RWS)*, pp.235,238, 15-18 Jan. 2012.

[35] R.-F. Xue, K.-W. Cheng, and M. Je, "High-Efficiency Wireless Power Transfer for Biomedical Implants by Optimal Resonant Load Transformation," *IEEE Trans. on Circuits and Systems I: Regular Papers*, vol. 60, no. 4, pp. 867 – 874, 2013.

[36] G. Monti, P. Arcuti, L. Tarricone, "Resonant Inductive Link for Remote Powering of Pacemakers," *IEEE Trans. on Microwave Theory and Techniques*, vol. 63, no. 11, pp.1-9, Nov. 2015.

[37] G. Monti, M. V. De Paolis, L. Tarricone, ''Wireless power transfer link for rechargeable deep brain stimulators," in *IEEE 15th Mediterranean Microwave Symp. (MMS)*, Lecce, Italy, 2015, pp. 1-4.

[38] G. Monti, M. V. De Paolis, L. Tarricone, ''Wireless energy link for deep brain stimulation," in *IEEE European Microwave Conference* (EuMC), Paris, France, Sept. 7-10, 2015, pp. 64-67.

[39] T. Campi, S.Cruciani, V. De Santis, et al., "EMF Safety and Thermal Aspects in a Pacemaker Equipped With a Wireless Power Transfer System Working at Low Frequency", *IEEE Trans. on Microw. Theory and Techn.*, vol. 64, no. 2, pp. 375-382, Feb. 2016.

[40] G. Monti, M. V. De Paolis, L. Corchia, M. Mongiardo, L. Tarricone, "Inductive Link for Power and Data Transfer to a Medical Implant," *accepted for publication in WPT Journal*, June 2016.

doi: 10.1109/MEMC.0.8339550

[41] M. Fu, C. Ma, X. Zhu, “A Cascaded Boost–Buck Converter for High-Efficiency Wireless Power Transfer Systems”, *IEEE Trans. on Industrial Informatics*, vol. 10, no. 3, pp. 1972-1980, 2014.

[42] M. D. Wei *et al*., "Balanced RF Rectifier for Energy Recovery With Minimized Input Impedance Variation," *IEEE Transactions on Microwave Theory and Techniques*, vol. PP, no.99, pp.1-7.

[43] K. Kotani, A. Sasaki and T. Ito, "High-Efficiency Differential-Drive CMOS Rectifier for UHF RFIDs," *IEEE Journal of Solid-State Circuits*, vol. 44, no. 11, pp. 3011-3018, Nov. 2009.

[44] Guideline, ICNIRP, “Guidelines for limiting exposure to time-varying electric, magnetic, and electromagnetic fields (up to 300 GHz)”, *Health Phys.*, vol. 74, no.4, pp. 494–522.

[45] Federal Communications Commission Office of Engineering & Technology OET Bulletin 65, “Evaluating Compliance with FCC Guidelines for Human Exposure to Radiofrequency Electromagnetic Fields,” Edition 97-01, August 1997.

[46] A. Costanzo, D. Masotti, “Energy-Harvesting Fabric Antenna”, chapter in book “Handbook of Smart Textiles”, Ed. Springer, pp. 1-22, March 2015.

doi: 10.1109/MEMC.0.8339550